Analyst

Accepted Manuscript

This article can be cited before page numbers have been issued, to do this please use: D. Liu, L. Zhou, L. Huang, Z. Zuo, V. Ho, L. Jin, Y. Lu, X. Chen, J. Zhao, D. Qian, H. Liu and H. Mao, *Analyst*, 2021, DOI: 10.1039/D1AN00464F.

ROYAL SOCIETY OF CHEMISTRY

rsc.li/analyst

View Article Online
DOI: 10.1039/D1AN00464F

View Article Online
DOI: 10.1039/D1AN00464F

Microfluidic integrated capacitive biosensor for C-Reactive Protein label-free and real-time detection

Dan-yang Liu[a,b,c]†, Lin Zhou[a,c,]†, Li-hong Huang[d,]†, Zhao-rui Zuo[e], Vincent Ho[f], Lai-di Jin[a,b,c], Yun Lu[b]， Xianfeng Chen[g], Jianlong Zhao [a,c], Dahong Qian[e,*], Hui-ying Liu[b,*] , Hong-ju Mao[a,c,*]

[a] Center of Materials Science and Optoelectronics Engineering, University of Chinese Academy of Sciences, Beijing 100049, China

[b] School of Stomatology, Dalian Medical University, Dalian 116044, China

[c] State Key Laboratory of Transducer Technology, Shanghai Institute of Microsystem and Information Technology, Chinese Academy of Sciences, Shanghai 200050, China

[d] The Second Affiliated Hospital of Dalian Medical University, Dalian 116027, China

[e] Institute of Medical Robotics, Shanghai Jiao Tong University, Shanghai 200240, China

[f] Richtek Technology Corporation, Taiwan, China;

[g] School of Electronic Engineering, Bangor University, Bangor LL57 1UT, UK

†These authors contributed equally to this work.

*Corresponding Authors:

Dahong Qian [e,] *, E-mail: dahong.qian@sjtu.edu.cn

Institute of Medical Robotics,

Shanghai Jiao Tong University,

No. 1954 Hua Shan Rd.

Shanghai, 200030, P.R. China.

Tel: +86-1391-818-2371

Fax: +86-02162511070-8714;

Hui-ying Liu [b,] *, E-mail: lhy04512000@dmu.edu.cn

School of Stomatology, Dalian Medical University,

9 Western Section, Lvshun South Street, Lvshunkou District,

View Article Online
DOI: 10.1039/D1AN00464F

Dalian 116044, P.R. China.

Tel: +86-41186110404;

Fax: +86-41186110397;

Hong-ju Mao [a, c]*, E-mail: hjmao@mail.sim.ac.cn

Chinese Academy of Sciences,

Shanghai Institute of Microsystem and Information Technology,

No.865 Changning Rd,

Shanghai 200050, P.R. China.

Tel: +86-02162511070;

Fax: +86-02162511070-8714;

View Article Online
DOI: 10.1039/D1AN00464F

Abstract

Microfluidic chip has been integrated with capacitive biosensor based on mass-producible three-dimensional (3D) interdigital electrode arrays. To achieve the monitoring of biosensor preparation and the cardiac and periodontitis-related biomarkers, all the processes were detected in a continuously on-site way. Fabrication steps for Microfluidic chip bonded 3D interdigital capacitor to monitor biosensor include gold thiol modification, the activation of EDC/sulfo-NHS, and the bioconjugation of antibodies. The fluorescent characterization and X-ray photoelectron spectroscopy analysis were applied to assess the successful immobilization of the C-Reactive Protein (CRP) antibody. The experimental results indicate the good specificity and high sensitivity of the Microfluidic integrated 3D capacitive biosensor. The limit of detection (LOD) of 3D capacitive biosensor for CRP label-free detection was about 1 $pg \cdot mL^{-1}$. This 3D capacitive biosensor with integrated Microfluidic is mass-producible and has achieved the on-site continuous detection of cardiac and periodontitis-related biomarkers with high performance.

Keywords: C-Reactive Protein; Capacitive biosensors; Microfluidic integration; Sulfhydryl modification; Electrochemical sensors; Biofunctionalization

1. Introduction

According to data from the World Health Organization (WHO), cardiovascular disease has become one of the leading causes of death globally [1],which posed a huge health threat and economic burden to the people. The risk of cardiovascular disease is always lurking in the development of the disease, and it may take several years to satisfy the diagnosis from sub-clinical state to clinical physical examination [2]. The risk factors for cardiovascular disease are usually evaluated by family history, cholesterol and blood pressure levels[3]. However, the above risk factors are not sufficient as prognostic tools to predict the risk of cardiovascular disease[4-6]. The current detection method is difficult to achieve dynamic evaluation of the patient's physiological status, disease risk, and feedback on the efficacy of medication[7, 8].

Biomarkers are a reliable and accurate auxiliary detection tool for screening

high-risk populations, predicting disease progression, and personalized diagnosis and treatment [9]. Cardiovascular disease biomarkers can help to carry out screening, diagnosis, and prognostic assessment of cardiovascular related diseases. The increased levels of various biomarkers in the serum are related to the risk of cardiovascular disease in patients. i.e., CRP[10, 11], interleukin-6 (IL-6) [12] and Brain natriuretic peptide (BNP) [10]. Among them, CRP is an acute-phase protein secreted by cells during the process of inflammation stimulation with a subunit molecular weight of about 20-30 kD and a total molecular weight of about 115 kD[13-15], which can cause adhesion molecules and inflammatory cells expression[16]. According to research, high CRP levels are associated with the risk of heart-related disease in patients with acute coronary syndrome[11]. In addition, as a biomarker, CRP plays an increasingly important role in the diagnosis of neonatal sepsis[17], microangiopathy[18] and cerebral embolism[19] .

The biomarkers contained in saliva participate in most physiological and pathological processes in the human body [20]. Reichert Stefan and others have found that severe periodontitis can lead to increased CRP levels in the blood [21], The concentration of CRP in blood is related to the concentration of CRP in saliva [22, 23]. At the same time, gingival crevicular fluid carries factors ingredients from serum and other components which related to oral microorganisms. Such as inflammatory mediators, antigens, etc. It can be collected noninvasively from the gingival sulcus or periodontal pocket by capillary action. Silvana P. Barros studies on biomarkers contained in gingival crevicular fluid indicate that gingival crevicular fluid has great research potential in disease diagnosis, prognosis and biomarkers[24]. Enzyme-linked immunosorbent assay (ELISA) is recognized as the standard method for the quantification of biomarkers in serum, which has been widely used in the detection of CRP[25]. The ELISA test method requires trained laboratory personnel to operate and has complex processes and high costs[26].

Biosensors can be used to detect biomarkers with high sensitivity[27]. Among them, fluorescent biosensors were proposed to CRP detection[28-30]. As an auxiliary method, fluorescent labeling runs through ELISA and other common detection

processes. But it can cause carcinogenic risk of fluorescent substances [31]. Improvements of label-based methods were urgently needed. It is well known that labeling is a time-consuming and high-cost process and may affect the interaction between receptor molecules and the analytes, especially regarding proteins [30]. Among different label-free biosensors, capacitive biosensors are noted for the ease of fabrication and signal readout, low power consumption, flexible sensor sizes, high sensitivity and the ability of integration of the readout circuits in the sensor. These features make capacitive biosensors meet the requirements of medical testing at point-of-care testing (POCT), in a doctor's office, a clinic, or even at home. Capacitive biosensors have ideal prospects for early diagnosis of diseases and potential disease risk detection[32].

Several capacitive biosensors based on miniaturized two-dimensional (2D) surfaces with immobilized biorecognition were reported to detect the related targets successfully [8, 33-35]. However, some limitations of 2D biosensors cannot be overlooked [36]. Firstly, the small surface area and surface area-to-volume ratio cause the reduced amount and therefore inefficient binding of specific targets and signal transduction, which may lead to instability of immobilized probes and low sensitivity. Moreover, the larger response time of 2D biosensors may be caused by the transportation diffusion, from analytes to the immobilized probe which only exists on a single surface. Furthermore, the effect of shear stress in a planar surface caused by sample loading can inhibit the bonding event between the analyte and the immobilized probe and will impose a significant impact on analytical performance.

In this work, the Microfluidic integrated mass-producible 3D interdigital capacitive biosensor was proposed to achieve the continuous on-site detection of cardiac and periodontitis-related biomarker with high performance. In order to reduce steric hindrance, the surface of the gold electrode is modified using mixed sulfhydryl molecules. The integrated Microfluidic channel for the capacitive sensor reduced the required sample amount for detection. In addition, the LCR instrument and the custom programs are used to set the detection experimental parameters and the real-time data acquisition, realizing the real-time monitoring of the capacitive biosensor's

bio-modification and target protein detection. The Microfluidic integrated 3D capacitive biosensors have been implemented to detect the specific CRP biomarkers as well as nonspecific biomolecules, demonstrating high sensitivity, real-time, specificity, and label-free sensing performance. This method may provide a powerful POCT tool for low-abundance protein detection, assist in the assessment of the risk of coronary heart disease and other cardiovascular diseases in clinical diagnosis, and broaden the application of oral non-destructive testing.

2. Material and methods

2.1. Reagents and instruments

Anti-CRP antibody, CRP antigen and myoglobin (MYO) antigen were purchased from Hytest Ltd. (Turku, Finland). Cytokeratin 19 (CK19) antigen and IL-6 antigen were purchased from Linc-Bio(Shanghai, China) and eBioscience Inc. (San Diego, USA),respectively.11-Mercaptoundecanoic acid, 6-Mercapto-1-hexanol, N-(3-Dimethylaminopropyl)-N′-ethyl carbodiimide hydrochloride (EDC), N-Hydroxysulfosuccinimide sodium salt (sulfo-NHS) and Streptomyces avidin (Cy3-SA) were got from Sigma (St. Louis, MO, USA). Phosphate-buffered saline (PBS, pH=7.2-7.4) were obtained from Sangon Biotech Co., Ltd. (Shanghai, China). Absolute ethanol were purchased from Lingfeng Chemical Reagent Co., Ltd. (Shanghai, China). Bovine Serum Albumin (BSA)was obtained from Equitech-Bio (Texas, USA). SU8 Negative Epoxy Resists was supplied by Kayaku Advanced Materials, Inc. (USA). Polydimethylsiloxane (PDMS) was obtained from Dow Corning Co., (NY, USA). BX51TRF microscope (Olympus Corporation, Japan) was used to characterize surface fluorescence modification of electrodes. X-ray photoelecgon spectroscopy (Thermo Fisher, USA) was used to verify the chemical modification of the electrodes. Precision LCR Meter E4980A (KEYSIGHT, USA) were used to measure the capacitive sensor. Millipore-Q purification system (Millipore, USA), was used to obtain deionized water for the preparation of all solutions. General serum diluent(GSD) were purchased from Immunochemistry Technologies (Minnesota, USA).

View Article Online
DOI: 10.1039/D1AN00464F

2.2 Fabrication of Microfluidic integrated 3D capacitive biosensors

The proposed 3D capacitive devices were fabricated by using the open cavity molding method based on the integrated circuit package lead frames[37]. After 3D interdigital electrodes were soldered on the printed circuit board (PCB), the BNC were assembled on both sides of PCB for the connection with the LCR instrument. The Microfluidic integrated 3D capacitive biosensor was fabricated as the following step. First, the SU8 photoresist was spin-coated onto the silicon wafer and patterned by photolithography. Second, the patterned silicon wafer may be step hard-baked between 170°C on a hot plate. Further, polydimethylsiloxane (PDMS) was prepared at a 10:1 (w/w) ratio of prepolymer to cross-linker and poured over the silicon master. After curing (incubation at 95°C for 1 h), the PDMS slab was peeled off and punched to create inlet/outlet ports. Finally, the PDMS slab was firmly bonded to an interdigital capacitive device by plasma treatment.

2.3 Biofunctionalization of 3D capacitive Biosensors

The integrated Microfluidic components provided low volume reagents for the construction of biosensor. Thiol mixtures, including 6-Mercapto-1-hexanol and 11-mercaptoundecanoic acid, were injected into the Microfluidic channel to functionalize 3D interdigital Au electrode arrays by utilizing syringe pump. The functionalization of different thiol molecules could improve accessibility for protein immobilization due to reduced steric hindrance[38]. Then, EDC and sulfo-NHS were used to activate the carboxyl group functionalized gold surface to form the ester group. Finally, CRP antibodies were introduced into the Microfluidic channel and incubated at room temperature to achieve the biofunctionalization of the 3D capacitive sensor.

2.4 Characterization of 3D biosensor surface functionalization

First, the fluorescent characterization of the 3D capacitive biosensor was applied to verify the successful immobilization of 11-mercaptoundecanoic acid by using streptavidin with Cy3. The fluorescence intensity of the 3D interdigital electrode was recorded by a fluorescence microscopy. Next, X-ray Photoelectron Spectroscopy

(XPS) analysis was used to characterize the surface composition of the functionalized gold electrodes in each step of the functionalization process. Thereafter, measurements of the dielectric parameters were performed at various steps of biosensor construction.

The capacitance change was recorded in each step of the functionalization process. The bio-functionalization process of 3D capacitive device includes: (a) Mixed thiol functionalization of gold electrode; (b) Carboxyl activation by EDC/sulfo-NHS; (c) Anti-CRP bioconjugation.

2.5 Measurements of the3D capacitive biosensor.

The Keysight LCR meter was applied to connect the 3D capacitive device and recorded the capacitance by utilizing the custom software for fully automatic multi-group testing on the computer. The capacitance changes of the 3D capacitive device based on the integration of Microfluidic channel and the injection of PBS buffer were measured by LCR meter. The specificity of the 3D capacitive biosensor was verified by monitoring the response under different protein solutions.

The different concentrations of CRP antigen were pumped into the microfluidic channel of integrated 3D capacitive biosensor, which changed the dielectric constant of 3D capacitive biosensor. The measurement system of the microfluidic chip integrated 3D capacitive biosensor was shown in Figure 1.

View Article Online
DOI: 10.1039/D1AN00464F

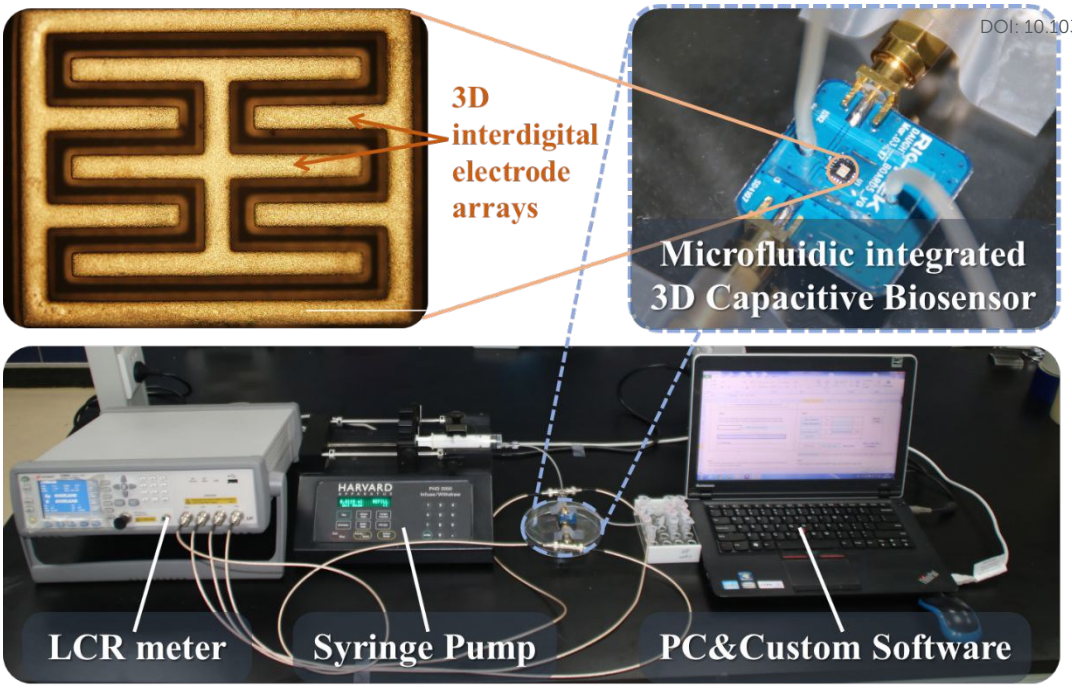

Figure 1: Micrograph of 3D interdigital electrode arrays (upper left), the photograph of Microfluidic integrated 3D capacitive biosensors (upper right) and the photograph of the measure system for the Microfluidic integrated 3D Capacitive Biosensor (lower).

3.Results & Discussion

3.1 Integration of Microfluidic chip and capacitive biosensor

Silicon wafers were photolithographically patterned using SU8-3050 photoresist. The steps are: Firstly, the SU8-3050 photoresist was spun on a silicon wafer at 1000 rpm. Secondly, The SU8-3050 photoresist coated wafer was baking on a hot plate. During the pre-baking, the temperature of the hot plate was set at 65 °C, and then the temperature of the hot plate was gradually increased to 95 °C at intervals of 5 °C. This baking process last for 45 min and the hot plate was turned off, then naturally cool it down to room temperature. Thirdly, the SU8-3050 photoresist coated wafer was exposed for 2 min. After the exposure, the photoresist coated was placed on a hot plate. After 5 min of post exposure bake at 95 °C, an image of microfluidic channel was visible on the surface of SU8 3050 photoresist. Turn off the power, and naturally cool it down to room temperature, and complete the post-baking step. After naturally cool to room temperature, the exposed silicon wafer was developed in Propylene

glycol methyl ether acetate (PGMEA) for 4 min. Finally, the resist was hard baked on a hot plate at 170 °C for 30 min to further cross-link the material.

To facilitate the bonding of the Microfluidic channel with the capacitor, a thin layer of PDMS was evenly applied on the PCB of the capacitor and cured in an oven for several minutes. Then the Microfluidic channel was bonded to the PDMS coated capacitor with 5 min plasma treatment. The integration of Microfluidic chip and capacitor and physical picture after red ink is injected into the Microfluidic channel were shown in FigureS1.

3.2 Construction of 3D capacitive biosensor

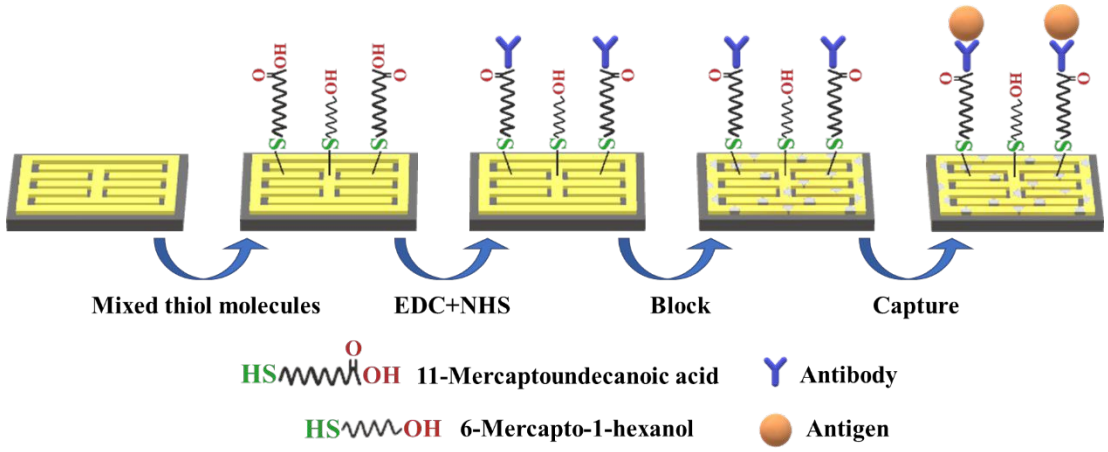

Figure 2 Schematic of functionalizing process of 3D capacitive biosensor.

The biofunctionalization of 3D capacitive biosensor was shown in Figure 2. Firstly, the mixed sulfhydryl molecules (11-Mercaptoundecanoic acid and 6-mercapto-1-hexanol) dissolved in absolute ethanol was injected into Microfluidic channels of the capacitor and incubated on the surface of the 3D interdigital electrode overnight. After finishing the uncombined sulfhydryl molecules were removed by absolute ethanol. The sulfhydryl groups of the mixed sulfhydryl molecules were bonded to the gold electrodes and at the same time 11-mercaptoic acid provided carboxyl group for the immobilization of anti-CRP. In addition, 6-mercapto-1-hexanol was used to increase the steric hindrance of the functionalized surface, which could enhance the efficiency of the functionalization of subsequent antibodies. Secondly, a mixture of 0.1 M EDC and 0.1 M sulfo-NHS solution was introduced into the surface of sulfhydryl functionalized 3D interdigital electrode. The

carboxyl groups on the surface of the gold electrodes were activated into an ester group.

After the completion of the above process stpes, the anti-CRPs solutions with the concentration of (100 ng·mL^{-1}) were injected into the integrated Microfluidic channel of the 3D capacitor and incubated for 1 hour. Then the unbound anti-CRPs were removed by the PBS. Finally, 10% BSA was added to block the free sites on the surface of the anti-CRP functionalized electrodes for 30 min. After the blocking process was completed, deionized water was injected into the Microfluidic channel to remove the remaining BSA molecules. All the functionalization processes were performed at room temperature. The prepared 3D capacitive biosensor was stored at 4 °C in the refrigerator.

3.3 Characterization of the gold electrode functionalization by XPS

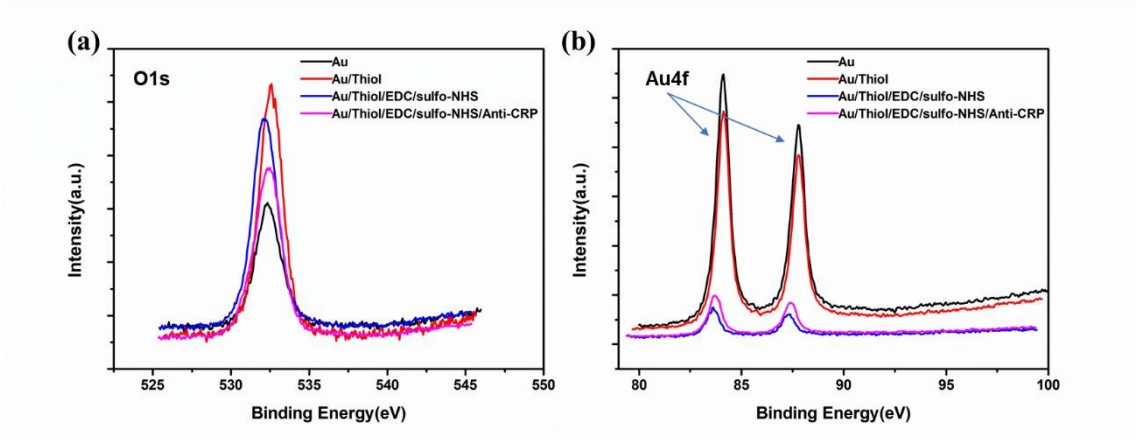

Figure 3(a) XPS O1s spectra of the bare gold electrode, mixed thiol molecules functionalized gold electrode, the treatment of EDC and sulfo-NHS and the immobilization of anti-CRP;(b) XPS Au spectra of the bare gold electrode, mixed thiol molecules functionalized gold electrode, the treatment of EDC and sulfo-NHS and the immobilization of anti-CRP.

The XPS analysis was utilized to explore the surface elements composition of the gold electrodes in each step of the functionalization process, including the bare gold electrode, mixed thiol molecules functionalized Au electrode, the treatment of EDC and sulfo-NHS and the immobilization of anti-CRP Au electrode.

The change of oxygen element during the surface functionalization of gold electrodes was recorded in Figure 3(a). After the self-assembly of mixed sulfhydryl

molecules, due to the carboxyl groups and hydroxyl groups of mixed sulfhydryl molecules, the peak of O1s shift from 532.32eV to 532.59eV and the intensity of this peak significantly increased. After the treatment of EDC and sulfo-NHS, the carboxyl group on the surface of the gold electrode was activated to an ester intermediate, and blue shift (about 0.52eV) was observed in the peak of O1s. Finally, after the immobilization of antibodies, the ester intermediate on the surface of the gold electrode was reacting with amine-containing anti-CRP, and the oxygen binding energy is found in the spectrum at 532.36eV. The amide bond formation led to lower the intensity of the peak of O1s as shown in Figure 3(a). XPS O1s spectra of Au electrode shown in Figure 3(a) indicated the successful immobilization of thiol mixture, EDC/sulfo-NHS and anti-CRP.

In addition, the XPS of the gold element was recorded in the bare gold electrode, mixed sulfhydryl molecules functionalized Au electrode, and the treatment of EDC/sulfo-NHS and the immobilization of anti-CRP, which was shown in Figure 3(b). While the surface of the gold electrode was gradually covered by the mixed sulfhydryl molecules and the EDC/sulfo-NHS, the intensity of the Au peak decreased gradually. Furthermore, the immobilization of anti-CRP was caused a slight increase in the intensity of the Au peak. All of these results demonstrated the obvious change in the coverage of the gold electrodes due to the biofunctionalization of 3D interdigital electrodes (as shown in Figure 3). Further , XPS Au spectra of Au electrode was about 83.6eV after the activation of EDC and sulfo-NHS and the immobilization of anti-CRP.

Mixed sulfhydryl molecules (6-Mercapto-1-hexanol and 11-mercaptoundecanoic acid) were introduced into the Microfluidic channel and incubated for 12 hours at room temperature. The change of nitrogen element during the surface functionalization of gold electrodes was recorded in Figure S2. The experimental results of XPS indicated the changes in surface element composition of 3D interdigital electrodes caused by the functionalization.

3.4 Fluorescent characterization of the biofunctionalization of gold electrodes

View Article Online
DOI: 10.1039/D1AN00464F

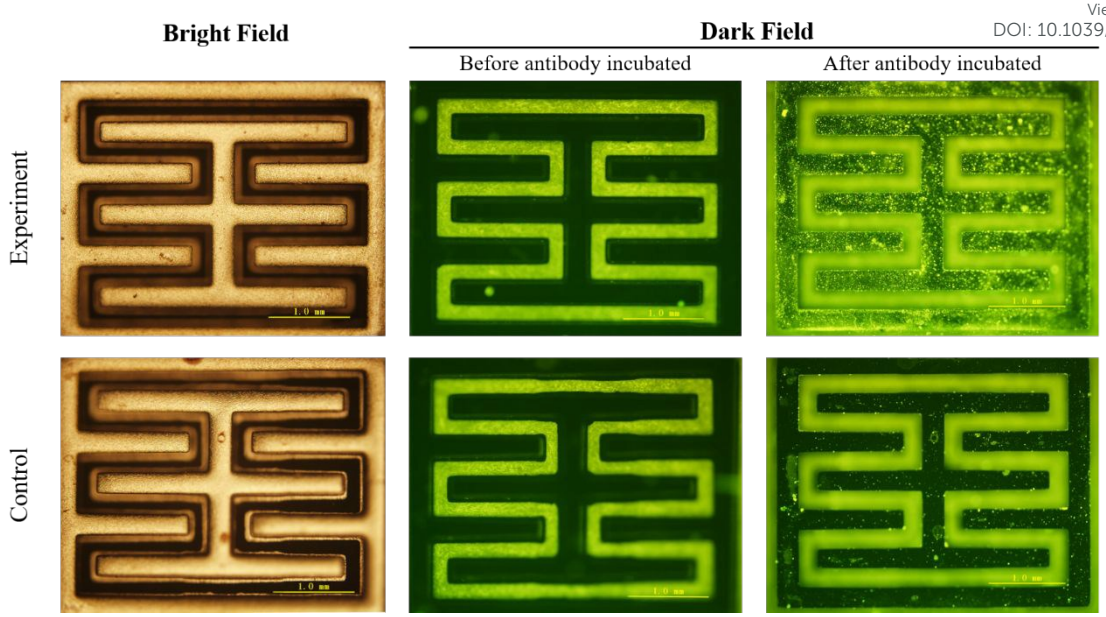

Figure 4 Fluorescent characterization of biofunctionalization of gold electrodes. Clustered fluorescent spots can be observed in the experiment group electrode photos after biological modification and antibody incubation. The dark field image of the control group electrode hardly changes before and after the antibody incubation.

To verify the immobilization of antibody via mixed sulfhydryl molecules and EDC/sulfo-NHS, streptavidin-Cy3 with the concentration of 1ug·mL^{-1} was injected into the surface of 3D gold electrodes after the activation of EDC and sulfo-NHS and incubated for 1 hour. In the experiment, photos of electrodes from the bright field and dark field, before and after biological modification were collected in the same channel and exposure time.

The experimental results were observed by comparing the electrode photos of the experimental group and the control group, as shown in Figure 4. Bright and clustered fluorescent spots can be observed in the electrode photos after biological modification and antibody incubation, despite of the fluorescence interference from the electrode gap. The fluorescence interference caused by the epoxy resin, which were used to package the 3D interdigital electrodes. At the same time, because the control group does not have a chemical group that can bind with the fluorescent antibody, the dark field image of the electrode showed little difference before and after the antibody incubation. The similar electrode images at a higher magnification of the microscope

were as shown in Figure S3. Fluorescent images of the functionalized gold electrodes indicated the effectiveness of biofunctionalization based on the mixed sulfhydryl molecules and EDC/sulfo-NHS.

3.5 Performance test of capacitive biosensors

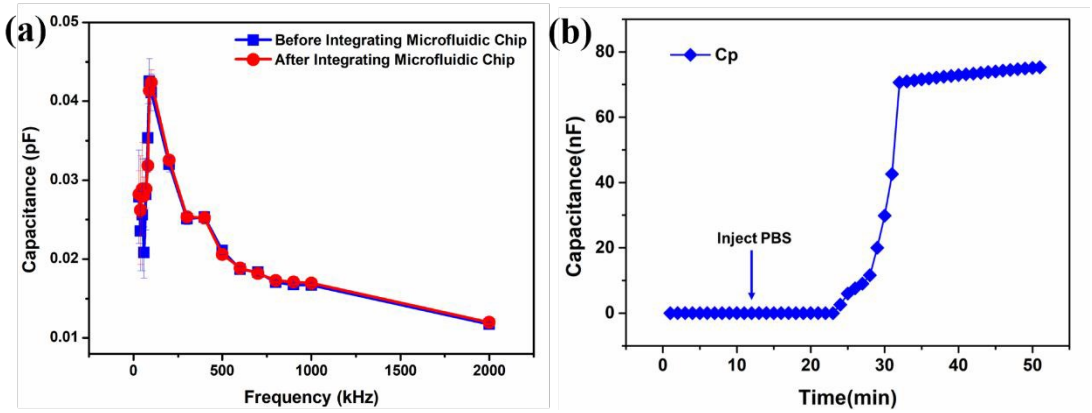

Figure 5(a) The capacitance of five 3D interdigital capacitors before and after integrating Microfluidic chip; (b) Capacitance changes before and after PBS injection.

Five different 3D capacitors were measured at the voltage of 0.1V under different frequencies. The capacitance of five devices decreased with the frequencies in Figure 5(a), which demonstrated the good consistency of these 3D interdigital capacitors. The measured capacitance of five devices before and after integrating Microfluidic chip in Figure 5(a) also indicated the Microfluidic chip bonding has little effect on the fluctuation of the capacitance data. After the integration of the Microfluidic chip, the capacitance was recorded during the PBS injection as shown in Figure 5(b).

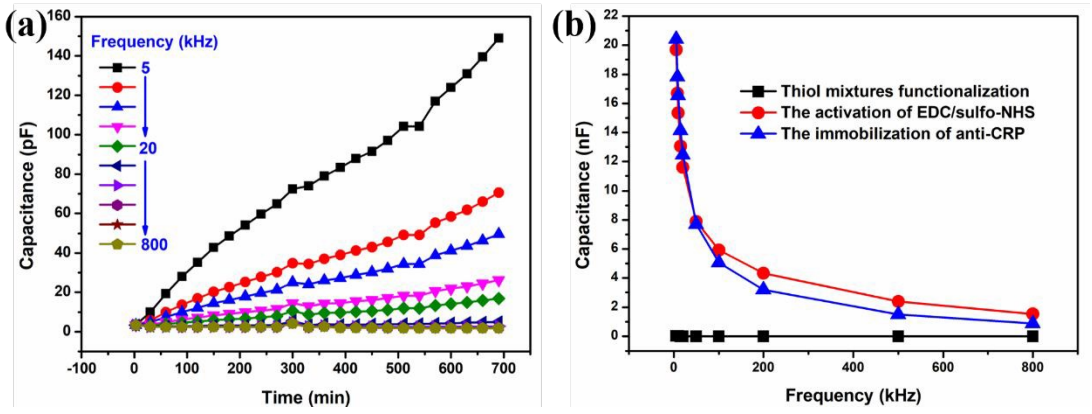

Figure 6 (a) The on-site monitoring of the thiol mixtures self-assembled on Au surface under

different frequencies; (b) The on-site monitoring of 3D interdigital capacitor after the treatment of the thiol mixtures, EDC/sulfo-NHS and anti-CRP.

Each step of the functionalization process of the gold electrodes was on-site monitored by the LCR meter. Figure 6(a) shows the bonding process between mixed sulfhydryl molecules and gold electrodes, the treatment of EDC/sulfo-NHS and the covalent binding of anti-CRP resulted in the change of the capacitance as is shown in Figure 6(b). The total molecular weight and surface charge of 3D interdigital electrodes after the biofunctionalization may influence the response of the capacitor biosensor, which need further investigate in the future work.

3.6 Specificity and sensitivity of Microfluidic integrated 3D capacitive biosensor

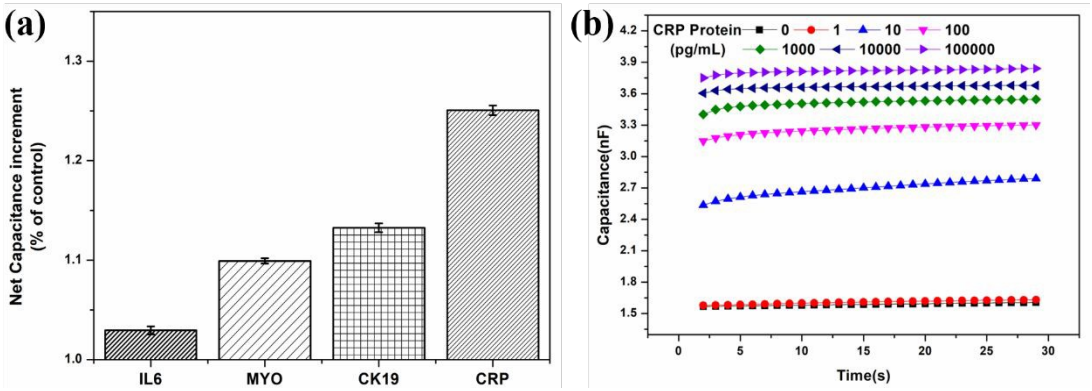

Figure 7 (a) Net capacitance responses to control group, CK19, MYO, IL-6, and CRP. (b) On-site continuous monitoring: the change of the capacitance value of the electric sensor as the CRP protein concentration increases.

To verify the specificity of the biosensor, CK19, MYO, IL-6 and PBS were injected into the Microfluidic channel as control groups. The concentration of all these proteins was 100 ng·mL-1. In particular, to avoid interfering with the interaction between the antigens, after each test of each antigen, the PBS buffer is introduced to wash the remaining reagent in the inlet and outlet tubes and the Microfluidic channel. The average value of the capacitance value obtained by the PBS test is used for data standardization, so as to obtain the analysis statistics of the capacitance increase in the specific test. The net capacitance increment verifies the specificity of the sensor, and the statistical result is shown in Figure7(a). The capacitance value of CRP antigen of

3D capacitive biosensors was obviously higher than that of control groups. Among them, the capacitance increases when interfering with protein detection may be caused by the non-specific adsorption of the protein on the electrode surface. It can be concluded that when antibody-antigen specific binding occurs on the sensor surface, the dielectric constant increases. In summary, the anti-CRP functionalized 3D capacitive biosensor exhibited high specificity for the detection of CRP.

To evaluate the sensitivity of the 3D capacitive biosensor, the CRP antigen solution dissolved in PBS buffer with 6 different concentrations (1, 10, 100,1000,10000,100000 pg·mL^{-1}) was injected into Microfluidic integrated 3D capacitor sequentially. The LCR meter controlled by custom software, set at the voltage of 200mV with different frequencies (from 20Hz to 1.5MHz). The capacitance values were real-time monitored by the LCR meter as shown in Figure 7(b). The capacitive values recorded by 3D capacitive biosensor were positively correlated with the concentrations of CRP antigen. The relationship between capacitance changes and CRP concentration (logarithm) is shown in Figure 8(a). As shown in this figure, based on the fitted curve, the correlation coefficient (R^2) was above 0.99, which indicates a high correlation between the curve and experiment results. The red line provides the best Langmuir model fitting of the experimental data. The Langmuir model is valid for monolayer sorption to a surface with a finite number of identical sites, which have been widely utilized in different biosensors [39-41].

These data were plotted to a nonlinear curve, indicating that the relationship between ΔF and the binding CRP could fit the Langmuir adsorption model described as follows:

$$\Delta F = \Delta F_{max} C_{\mathrm{crp}} / (K_d + C_{\mathrm{crp}})$$

Where K_d is the dissociation constant of the interaction between CRP and anti-CRP, $C_{crp}$is the protein concentration, ΔF_{max} is the saturated capacitance and Δ Fdenotes net capacitance value. According to the fitting results, the value of saturated capacitance ΔF_{max} was calculated to be about 2.12nF. The dissociation constant (K_d) of the interaction between the anti-CRP antibody and CRP can be estimated by measuring the capacitance at different CRP concentrations, which was estimated to be

0.024 ng·mL^{-1}. The limit of detection (LOD) of 3D capacitive biosensor was estimated by the total of the means of the blank response and 3 times standard deviation of the blank response.

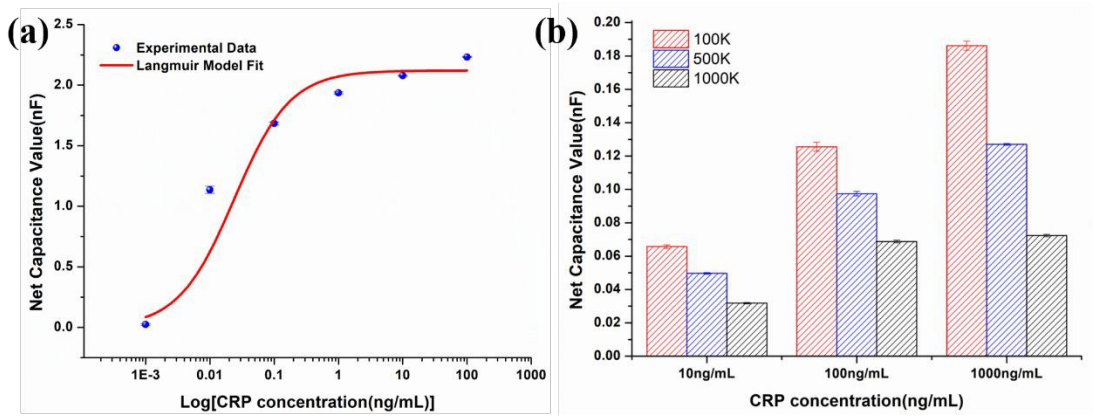

Figure 8 (a) Label-free detection of CRP with anti-CRP immobilized 3D capacitor, the red line is the best Langmuir model fit curve; (b) Net capacitance increment with different CRP concentrations in diluted serum sample under different capacitor working frequencies.

3.7 Detection with the serum sample

The clinical serum sample with known CRP concentrations (tested by ELISA kit) were utilized to validate the performance of this integrated capacitive biosensor. Due to the high CRP concentration in this sample (the level of micrograms per milliliter) and the high viscosity of serum sample (which may block the microfluidic channel), GSD was chosen as a dilution reagent to dilute the CRP concentration in the sample to several specified concentrations (10,100,1000ng·mL^{-1}). The diluted serum was measured by this integrated 3D capacitive biosensor with different capacitor working frequencies (100kHz, 500kHz and 1000kHz), as shown in Figure 8(b). The average of capacitance values obtained from the detection of GSD solution is used for data normalization. As working frequencies increased, the response difference of this biosensor at different concentrations decreased obviously, which indicated the lower working frequency was more suitable for biomolecules detection.

As the similar responses of this integrated 3D biosensor in PBS, the capacitance increased with the CRP concentration in the serum sample. The experimental results could be also fitted with the Langmuir model and the details information about the

calculated parameters was shown in Figure S4. The stable and effective responses in serum of this integrated 3D biosensor means the possibility of clinical application for this biosensor. The difference responses in PBS and serum for this biosensor may attributed to the adsorption of unspecific biomolecules in the complex serum samples.

4.Conclusions

The proposed fully symmetric 3D interdigital electrode arrays were fabricated by using the open cavity molding method based on the integrated circuit package lead frames. The Microfluidic components has been integrated with 3D capacitive biosensor to create low sample required and surface shear stress controllable sensing devices with the aid of the syringe pump. The 3D interdigital Au electrode arrays were modified by various thiol mixtures of 6-Mercapto-1-hexanol and 11-mercaptoundecanoic acid, the results of XPS and fluorescent characterization of the biofunctionalized gold electrodes indicated the successful immobilization of Anti-CRP. Different concentrations of CRP protein in PBS and diluted serum were injected into the integrated microfluidic channel by a syringe pump, which were continuously monitored by the LCR meter. The LOD of this integrated 3D capacitive biosensor could reach 1pg·mL^{-1} in PBS. The effective responses in serum of this integrated 3D biosensor provided the possibility of clinical application for cardiovascular and periodontitis-related biomarkers detection.

Credit authorship contribution statement

Dan-yang Liu: Conceptualization, Investigation, Validation, Analysis, Writing - original draft. Lin Zhou: Conceptualization, Methodology, Investigation, Writing-original draft, Review & Editing. Li-hong Huang: Resources, Formal analysis. Zhao-rui Zuo: Software. Vincent Ho: Methodology. Lai-di Jin: Data Curation. Yun Lu: Formal analysis. Xianfeng Chen: Review, Discussion & Revision Suggestions. Dahong Qian: Review & Editing - original draft. Jianlong Zhao: Review, Discussion & Revision Suggestions. Hui-ying Liu: Supervision, Review & Editing - original draft, Funding acquisition. Hong-ju Mao: Project administration, Review & Editing - original draft, Funding acquisition.

View Article Online
DOI: 10.1039/D1AN00464F

Acknowledgements

This work was supported by National Key Research and Development Program of China (No. 2018YFA0108202 and 2017YFA0205300), National Natural Science Foundation of China (Grant number: 61871068, 61971410, 61801464, 61801465, 81801016 and 61701171), the Science and Technology Commission of Shanghai Municipality (Nos. 19511104200), Department of Science and Technology of Zhejiang Province - Key Research and Development Program(2017C03029).

Highlights

Microfluidic chip integrated capacitive biosensor platform based on mass-producible three-dimensional (3D) interdigital electrode arrays.

Achieved continuously on-site monitoring during preparing biosensor biofunctionalization and detecting the biomarker.

The mixed thiol molecules are used to carboxylate the electrode surface to reduce the steric hindrance during antibody binding.

References

1. WHO, http://www.who.int/mediacentre/factsheets/fs317/en).
2. J. E. Ho, A. Lyass, P. Courchesne, G. Chen, C. Liu, X. Yin, S. J. Hwang, J. M. Massaro, M. G. Larson and D. Levy, *Journal of the American Heart Association*, 2018, **7**.
3. A. J. G. Lemos, R. P. A. Balvedi, V. R. Rodovalho, L. O. Resende, A. C. H. Castro, S. Cuadros-Orellana, J. M. Madurro and A. G. Brito-Madurro, *Microchemical Journal*, 2017, **133**, 572-576.
4. J. H. Ware, *The New England journal of medicine*, 2006, **355**, 2615-2617.
5. R. Nangia, H. Singh and K. Kaur, *Medical journal, Armed Forces India*, 2016, **72**, 315-319.
6. R. Dhingra and R. S. Vasan, *Trends in cardiovascular medicine*, 2017, **27**, 123-133.

7. A. Qureshi, Y. Gurbuz and J. H. Niazi, *Sens. Actuator B-Chem.*, 2012, **171**, 62-76.
8. S. Szunerits, V. Mishyn, I. Grabowska and R. Boukherroub, *Biosens. Bioelectron.*, 2019, **131**, 287-298.
9. R. S. Vasan, *Circulation*, 2006, **113**, 2335-2362.
10. A. May and T. J. Wang, *Trends in molecular medicine*, 2008, **14**, 261-267.
11. R. J. de Winter, R. Bholasingh, J. G. Lijmer, R. W. Koster, J. P. Gorgels, Y. Schouten, F. J. Hoek and G. T. Sanders, *Cardiovasc Res*, 1999, **42**, 240-245.
12. P. M. Ridker, *Circulation Research*, 2016, **118**, 145-156.
13. A. Pathak and A. Agrawal, *Front Immunol*, 2019, **10**, 943-943.
14. A. K. Shrive, G. M. T. Gheetham, D. Holden, D. A. A. Myles, W. G. Turnell, J. E. Volanakis, M. B. Pepys, A. C. Bloomer and T. J. Greenhough, **3**, 346-354.
15. S. De Servi, M. Mariani, G. Mariani and A. Mazzone, *Journal of the American College of Cardiology*, 2005, **46**, 1496-1502.
16. B. Lindahl, H. Toss, A. Siegbahn, P. Venge and L. Wallentin, *The New England journal of medicine*, 2000, **343**, 1139-1147.
17. D. Sharma, N. Farahbakhsh, S. Shastri and P. Sharma, *J Matern Fetal Neona*, 2018, **31**, 1646-1659.
18. M. P. Hermans, S. A. Ahn and M. F. Rousseau, *Journal of Diabetes and its Complications*, 2019, **33**, 107413.
19. M. Tsushima, N. Metoki, J. Hagii, S. Saito, H. Shiroto, M. Yasujima, T. Kato, N. Kudo, Y. Toyama, Y. Yokono, M. Nozaka, Y. Kawamura, M. Nakata and H. Tomita, *Journal of Stroke and Cerebrovascular Diseases*, 2019, DOI: https://doi.org/10.1016/j.jstrokecerebrovasdis.2019.104534, 104534.
20. A. R. Saad, K. Zohaib, H. N. Fayez, N. Mustafa, A. W. Hamed, S. Haafsa and S. K. Rabia, *Proteomes*, **5**, 21-.
21. S. Reichert, L. Seitter, H.-G. Schaller, A. Schlitt and S. Schulz, *Cytokine*, 2020, **127**, 154932.
22. C. S. Miller, J. D. Foley, A. L. Bailey, C. L. Campell, R. L. Humphries, N.

Christodoulides, P. N. Floriano, G. Simmons, B. Bhagwandin, J. W. Jacobson, S. W. Redding, J. L. Ebersole and J. T. McDevitt, *Biomark. Med.*, 2010, **4**, 171-189.

23. A. Mohd. Khairuddin Md, F. Mohamad Faris Bin Mohamad, C. B. G. Subash, A. R. Ruslinda, N. Mohammad Nuzaihan Md, L. Hong Yoong and H. Uda, *Current Medicinal Chemistry*, 2016, **23**, 4270-4284.
24. S. P. Barros, R. Williams, S. Offenbacher and T. Morelli, *Periodontol 2000*, 2016, **70**, 53-64.
25. S. L. Navarro, E. D. Kantor, X. Song, G. L. Milne, J. W. Lampe, M. Kratz and E. White, *Cancer epidemiology, biomarkers & prevention : a publication of the American Association for Cancer Research, cosponsored by the American Society of Preventive Oncology*, 2016, **25**, 521-531.
26. G. J. Zhang and Y. Ning, *Anal Chim Acta*, 2012, **749**, 1-15.
27. L. Zhou, K. Wang, H. Sun, S. Zhao, X. Chen, D. Qian, H. Mao and J. Zhao, *Nano-Micro Letters*, 2019, **11**, 20.
28. J. Pultar, U. Sauer, P. Domnanich and C. Preininger, *Biosens Bioelectron*, 2009, **24**, 1456-1461.
29. P. Salvo, V. Dini, A. Kirchhain, A. Janowska, T. Oranges, A. Chiricozzi, T. Lomonaco, F. Di Francesco and M. Romanelli, *Sensors (Basel)*, 2017, **17**, 2952.
30. J. Hu, Z.-L. Zhang, C.-Y. Wen, M. Tang, L.-L. Wu, C. Liu, L. Zhu and D.-W. Pang, *Analytical chemistry*, 2016, **88**, 6577-6584.
31. M. F. Fathil, M. K. Md Arshad, A. R. Ruslinda, M. N. M. Nuzaihan, S. C. Gopinath, R. Adzhri and U. Hashim, *Anal Chim Acta*, 2016, **935**, 30-43.
32. V. Tsouti, C. Boutopoulos, I. Zergioti and S. Chatzandroulis, *Biosens Bioelectron*, 2011, **27**, 1-11.
33. A. J. Steckl and P. Ray, *Acs Sensors*, 2018, **3**, 2025-2044.
34. R. N. Dalila, M. K. M. Arshad, S. C. B. Gopinath, W. M. W. Norhaimi and M. F. M. Fathil, *Biosens. Bioelectron.*, 2019, **132**, 248-264.
35. O. Parlak, A. İncel, L. Uzun, A. P. F. Turner and A. Tiwari, *Biosens.*

View Article Online
DOI: 10.1039/D1AN00464F

Bioelectron., 2017, **89**, 545-550.

36. R. Rebelo, A. I. Barbosa, D. Caballero, I. K. Kwon, J. M. Oliveira, S. C. Kundu, R. L. Reis and V. M. Correlo, *Biosens. Bioelectron.*, 2019, **130**, 20-39.
37. Z. R. Zuo, K. Wang, L. B. Gao, V. Ho, H. J. Mao and D. H. Qian, *Sensors*, 2019, **19**, 12.
38. J. W. Lee, S. J. Sim, S. M. Cho and J. Lee, *Biosens. Bioelectron.*, 2005, **20**, 1422-1427.
39. K. Wang, L. Zhou, Z. S. Wang, Z. L. Cheng, H. D. Dong, Z. H. Wu, Y. N. Bai, Q. H. Jin, H. J. Mao and J. L. Zhao, *Sens. Actuator B-Chem.*, 2018, **258**, 558-565.
40. Y. Saylan and A. Denizli, *Sensors (Basel)*, 2018, **18**.
41. J. C. Soares, A. C. Soares, P. A. Pereira, C. Rodrigues Vda, F. M. Shimizu, M. E. Melendez, C. Scapulatempo Neto, A. L. Carvalho, F. L. Leite, S. A. Machado and O. N. Oliveira, Jr., *Physical chemistry chemical physics : PCCP*, 2016, **18**, 8412-8418.